ELSEVIER

Journal of Molecular Catalysis A: Chemical 102 (1995) 175–191

JOURNAL OF MOLECULAR CATALYSIS A: CHEMICAL

# Kinetic method for the characterization of Brønsted sites on oxide surfaces. Part I. Trimethylorthobenzoate hydrolysis over a series of $Al_2O_3/SiO_2$ mixed oxides

Vlad T. Popa [1], Cristian Contescu[1], James A. Schwarz *

*Department of Chemical Engineering and Materials Science, Syracuse University, Syracuse, NY 13244-1190, USA*

Received 17 February 1995; accepted 15 May 1995

**Abstract**

The hydrolysis of trimethylorthobenzoate was studied over the pH range 4–7. In homogeneous experiments, overall first-order kinetics was found for both constant and variable proton concentrations, with an average intrinsic rate constant of $6 \cdot 10^3$ l/mol·min. Within the above pH range, it was also found that a series of alumina/silica oxides could act as general catalysts for the same reaction. Proton binding on the oxides determined from potentiometric titration data revealed two types of potentially active, proton-donor, sites with acid strengths $pK_a^I \approx 4$ and $pK_a^{II} \approx 5.5$. A detailed kinetic analysis is presented which accounts for the time dependent mass, charge and site balance in the system. Kinetic scanning, which involves a pH perturbation and subsequent analysis of the heterogeneous system relaxation, is proposed as a general method for evaluation of the concentration of surface sites active for general acid catalysis. Active site densities, determined by means of this approach, increased from 0.085 to 0.13 mmol/g as the aluminum content in the mixed oxides increased from 3 to 10% by weight. The proton transfer rate constant's value, essentially independent of oxide composition, was estimated at $\approx 1500$ g/mol·min.

*Keywords*: Acid catalysis; Proton affinity distributions; Proton transfer; Variable pH kinetics

## 1. Introduction

The general concept of catalyst heterogenization is to disperse on a more or less inert support a catalyst whose activity has been identified in the homogeneous phase. Synergistic effects are expected, but antagonistic ones are not excluded if the overall catalytic activity is not the simple superposition of the action of the active phase and that of the support. A recent monograph [1] appropriately recounts the old practice of using chemical kinetics as a discriminator in such instances: 'The definition of a catalyst rests on the idea of reaction rate, and therefore the subject of reaction kinetics is central, providing the quantitative framework. The qualitative chemical explanations of catalysis take the form of reaction mechanisms. These are models of reactions accounting for the overall stoichiometry, identifying the sequence of elementary reaction steps, and (insofar as possible) explaining, in terms of chemical bond strength and geometry, the interactions of the catalyst with reactants.'

Solid oxides are a convenient vehicle for the 'heterogenization' of the proton, a well-known

* Corresponding author.

[1] Permanent Address: Institute of Physical Chemistry, Spl. Independentei 202, Bucharest 77208, Romania.


*SSDI* 1381-1169(95)00103-4

homogeneous catalyst. Proton transfer in both homogeneous and heterogeneous systems is a widespread notion in the literature of the last seven decades, starting with Brønsted's theory [2]. Fundamental monographs such as those of Bell [3], Caldin and Gold [4] or more recently that by Stewart [5] summarize the huge amount of published contributions, pertaining merely to organic reactions. Solids acting as acid–base catalysts have been progressively developed within this field in connection with their exhibited superacidity (far less their superbasicity) in nonaqueous media [6]. Strong acid properties of simple and mixed oxides have proven to be responsible for their catalytic properties in conventional gas–solid contact catalysis [1] in a large number of reactions for which aqueous environments are generally considered to have a detrimental effect. This is due to both the ampholytic 'leveling action' of water (which cancels strong acid surface sites) and to its high sorption affinity on oxides, collectively resulting in 'poisoning' the catalyst surface. The reverse is also true for other types of reactions, water being responsible for the conversion of inactive Lewis into active Brønsted sites [7]. Although the aqueous–solid interface and its binding properties with respect to organic compounds have been the subject of detailed investigations, commonly in connection with soil chemistry and pollution [8], studies concerning the acid catalytic properties of oxides in aqueous media are not so prevalent.

Recently a specific method to evaluate proton adsorption equilibria at the solid–water interface was described [9]; it offers a means of characterizing solid samples, under conditions similar to those in which catalysts are prepared, from the point of view of their proton transfer to the surrounding aqueous medium. The method was applied to various oxide and mixed oxide materials [10] and its extension is in progress [11]. In accordance with our improved understanding of proton binding/release to/from solids, this current work was initiated to answer the question: Do the proton transfer properties of various surface sites as determined from aqueous (quasi)-equilibria manifest themselves in the presence of an organic substrate acceptor able to undergo an acid–base catalyzed reaction? Silica and silica–alumina were selected, as their interface exhibits an acidic strength similar to carboxylic acids and allow us to adopt an approach related to homogeneous catalysis. The hydrolysis of an orthoester (trimethyl orthobenzoate) was selected in view of its well-established homogeneous mechanism.

The problem we try to solve is that of separating the (homogeneous) specific and (heterogeneous) general catalysis contributions [1,3–5]. However, unlike homogeneous catalysis, where the precise determination of the general catalyst concentration and constant pH conditions are easily achieved via appropriate buffers, oxide equilibration in aqueous media is generally very slow [8] resulting in a variable pH solution, at least within the time-scale of the kinetic measurements. Moreover, the general acid concentration, that is the surface acid site density, is an unknown quantity requiring separate experiments for its evaluation. Stable pH is therefore far more difficult to attain with heterogeneous systems and the use of buffers would even complicate the problem of separating the (general acid) contribution of the solid catalyst. Our solution was to take advantage of this phenomenon and deliberately impose a variable pH within an experimental setup bearing some resemblance to non-steady thermal analysis techniques. Thus we performed a 'kinetic scan' of the hydrolysis reaction simultaneously with a study of surface proton-donor properties.

The developed experimental method and kinetic analysis are by no means restricted to the selected test reaction and solid acids. Their extension is open to a broader class of acid–base homogeneously and heterogeneously catalyzed reactions, subject to the constraint (easy to fulfill experimentally) that a reactant excess ensures overall pseudo first-order kinetics.

## 2. Experimental

### 2.1. Materials

All chemicals were certified reagents from Aldrich or Fisher Scientific and were used without further purification. Silica and alumina/silica samples were prepared by the sol–gel/xerogel method [12] from tetraethylorthosilicate (98+%) and aluminum isopropoxide (98%); deionized water and spectrophotometric grade ethyl alcohol were also used in obtaining the corresponding gels. These were first dried at 110°C for 16 h, then calcined at 600°C for 10 h, in ambient atmosphere. After grinding and sieving, the 40–80 mesh fraction was selected for all subsequent measurements. The compositions of the different samples were respectively 10, 7 and 3% (weight percent) $Al_2O_3$. The inert electrolyte was prepared from A.C.S. sodium nitrate and deionized water. Certified volumetric standard solutions (0.1 N nitric acid and 0.1 N sodium hydroxide) were used as received, as well as the electrode calibration buffers (pH 4.00, 7.00 and 10.00). Trimethylorthobenzoate 98% (Aldrich) was used as the hydrolysis substrate.

### 2.2. Potentiometric titration

The experimental setup was essentially the same as the one previously reported [9]. Titrants were accurately ($\pm 0.001$ ml) dosed by means of a 665 Dosimat (Metrohm) microburet which served in both jump and continuous pH-drift experiments. The pH was measured by means of a digital Fisher Scientific pH/Ion/Conductivity Meter Accumet Model 50 with Standard Glass-Body Combination Electrode (Fisher #13-620-271 with calomel reference) and the instrument output was stored automatically with sampling rates between one and six points per minute, depending on the pH variation rate. A protective nitrogen purge (50 ml/min) provided the inert atmosphere for both titration and kinetic runs; the measured solutions were thus free of oxygen and carbon dioxide that could affect the hydrolysis reaction and the potentiometric titration whose description was given previously [9] and will not be presented here.

As previously shown [9–11] the proton affinity distributions enable qualitative and quantitative analysis of acid–basic surface sites. They were used for the evaluation of both $K_a$ (for quasi-equilibrated proton desorption–adsorption) and surface site concentration.

### 2.3. Reaction kinetics

The time course of the reaction was followed by means of a Bausch&Lomb Spectronic 1001 spectrophotometer with a thermoelectric flowcell accessory. The solution volume was fixed at 50 ml, out of which approximately 1ml (0.5 ml for the spectrophotometer cell + $\approx$0.5 ml for the glass frit and peristaltic pump tubing) formed the measuring loop which was devised as a small recirculating system attached to the reaction vessel. The typical sampling rate for kinetic runs was fixed to three points per minute; a small delay between successive pumpings avoided the perturbations caused by bubbles formed due to the frit's partial clogging during heterogeneous experiments. Magnetic stirring ensured the liquid phase homogeneity and a quasi-uniform repartition of the solid-phase particles within the reaction space while thermostated jacketed beakers provided temperature stability at the selected value of $25 \pm 0.1$°C.

The absorbance of benzoic acid was followed at 270 nm, where some interference of $NO_3^-$ occurs, but only as a constant background. The overall absorbance level (referenced to deionized water taken as zero) was kept below 2 by means of both inert electrolyte concentration ($NaNO_3$, 0.1 N) and the quantity of organic reagent. The latter was dosed with a Hamilton Gastight #1801 syringe; after preliminary testing and calibration the injected volume was fixed at 5 $\mu$l.

Homogeneous (HOM) and heterogeneous (HET) experiments were performed under identical conditions. In HET runs solid catalyst weights were $0.102 \pm 0.001$ g. Constant pH runs

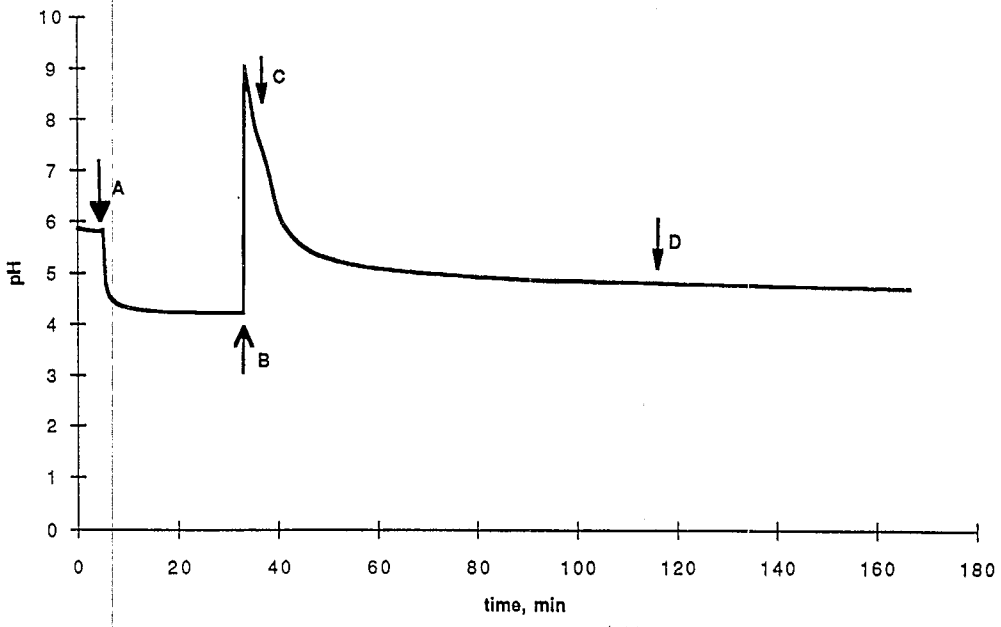


Fig. 1. pH–time pattern of a 10% $Al_2O_3/SiO_2$ HET run.

involved, in both HOM and HET modes, reaching a stable pH reading after the addition of basic titrant. This readily occurred in the first case, while in the second one the equilibration process was much slower, mainly due to the lower rate of the surface protonation–deprotonation processes that take place [12]. To avoid the involvement of the bulk solid in such processes [13], the equilibration waiting period was not more than 40 min and a constant pH run was considered one in which the pH variation did not exceed 0.1 units over the whole reaction duration. As a pH drift always took place in HET runs, we decided to perform the hydrolysis reaction even under these conditions and eventually take advantage of the pH variation by means of some suitable mechanistic modeling and data processing.

All samples investigated exhibited acidity upon immersion in the aqueous reaction medium, which is the expected behavior of silica and silica–alumina materials [14]. At the corresponding (quasi)equilibrium pH values (lying below 4.4 for samples weights around 0.1 g) the reaction rate is too high and even with the maximum allowable sampling rate reliable data acquisition is impossible. As explained in detail in the following section at such pH values the heterogeneous contribution to the catalytic act is negligible as the reaction 'chooses' the more facile homogeneous route. The medium acidity was lowered through sodium hydroxide addition thus forcing the reaction to 'seek' for the (weak) surface acid sites of the solid catalyst. A series of experiments consisted in monitoring the reaction at some stable pH reached after base addition and system equilibration. Another series made use of the pH-jump technique by following the time course of surface protonation–deprotonation relaxation and hydrolysis reaction concomitantly.

A typical pH-jump experiment is depicted in Fig. 1, which contains the pH evolution pertaining to the 10% $Al_2O_3/SiO_2$ sample. Five minutes after the start of the recording the solid is introduced into the electrolyte solution (point A). The initially steep pH fall is followed by a long 'tail' with slow variation. After 30 min (point B), 0.1 N NaOH solution (volume between 50 and 250 $\mu$l, depending on the sample and the desired final pH value) is provided by the microburet. The first injection of organic reagent (C) occurs within the fast decreasing region following the pH jump, whereas the second (D) takes place somewhere in the flat, 'quasi-constant' pH range, after the complete consumption of the initial amount. The

above stand for 'variable pH runs' and 'constant pH runs'. For a series of constant pH runs only the second injection was done and the transient domain was disregarded. It should be emphasized that absolute pH constancy was not attained neither in simple nor in combined (Fig. 1) heterogeneous kinetic experiments. For the HOM runs a similar pH variation was produced by adding acid (5 $\mu$l/min) following an initial pH jump.

Trimethylorthobenzoate was chosen in view of numerous older [15] and more recent [5] studies, reporting the homogeneous hydrolysis of this substrate as occuring in general acid catalysis and thus allowing for direct implication of the solid in the catalytic act. This clearly differentiates the present study from a previous attempt [16] in which acetals (hydrolysis in specific acid catalysis) were used as 'kinetic markers' for the evaluation of solid acidity.

## 3. Kinetic analysis

The trimethylorthobenzoate hydrolysis reaction,

$$C_6H_5C(OCH_3)_3 + 2H_2O \rightleftharpoons C_6H_5COOH + 3CH_3OH$$

is assumed to take place both homogeneously and heterogeneously, catalyzed in a specific manner by the hydrated proton and in a general one by the surface (weak) acid sites. Separation of the two reaction routes is essential from the point of view of the kinetic analysis. In the presence of a large excess of water, first-order kinetics is expected and actually found throughout the experimental range investigated.

The '$A_1$' mechanism [3–5,15] was taken as valid for the homogeneous contribution. Within the framework of a two-step sequence, it assumes first the quasi-equilibrated protonation of the substrate, A, followed by a rate determining, unimolecular decomposition of the intermediate formed, with subsequent steps fast and thus kinetically insignificant:

$$(1)\ A + H \rightleftharpoons AH;\ K_0 = \frac{[A][H]}{[AH]}$$

$$(2)\ AH \rightarrow \ldots \text{prod};\ k_0$$

In the above and what follows, H stands for the hydrated proton, square brackets for concentrations, $K_0$ is the acidity constant of the protonated intermediate and $k_0$ designates the rate determining step (rds) rate constant; the charge signs are omitted for convenience. The homogeneous reaction rate reads:

$$r_{hom} = -d[A]/dt = k_0[AH]$$
$$= (k_0/K_0)[H][A] = k_{hom}[H][A] \quad (1)$$

In terms of the measured absorbance, $a$, the integrated form of Eq. 1 is given by:

$$\ln\beta = k_{hom}[H](t-\tau) = \kappa_{hom}(t-\tau);$$
$$\beta = \beta(t) = [a(\infty) - a(\tau)/[a(\infty) - a(t)] \quad (2)$$

where $\tau$ is the time lag required for the complete dispersion of reactant, $a(\infty)$, $a(\tau)$ and $a(t)$ are absorbance readings at reaction end (endpoint), $\tau$ and current time, $t$, respectively; $\kappa_{hom}$ is the observed homogeneous first order rate constant. Eq. 2 holds for constant pH runs. For variable pH, if the [H] variation rate is not too high so that step (1) of the above sequence can still be assumed in quasi-equilibrium and denoting by $h(t)$ the time-dependent proton concentration, the rate expression becomes:

$$r_{hom} = -(d[A]/dt)_{hom} = k_{hom}[A](t)h(t) \quad (3)$$

which yields, on integration:

$$\ln\beta = k_{hom}\int_{\tau}^{t} h(t)\,dt = k_{hom}H(t) \quad (4)$$

The quantity $H(t)$, which could be termed the 'proton integral', can be accurately computed from pH readings, provided a suitable sampling rate is used. A plot of $\ln\beta$ versus $H(t)$ thus gives $k_{hom}$, the 'intrinsic' (second order), as opposed to $\kappa_{hom}$, the 'apparent' rate constant. This procedure is similar to the 'replacement of time with an area

variable' [17] of French [18] and Wideqvist [19] (second-order kinetics) with the notable difference that here the time variation of the homogeneous catalyst concentration is taken into account. If $h(t) = \text{const}$ Eq. 4 yields Eq. 2, so that it can be used for determining $k_{hom}$ for both constant and variable pH runs.

For the heterogeneous route, we assume that proton transfer from surface sites (hydroxyl groups) to the substrate is the slow step. This is reasonable, due to the much lower 'bulk' mobility of the surface protons compared to that of the solvated ones, as well as to the need of overcoming the double layer barrier [4–8]. This assumption is also consistent with the picture viewing the solid surface acting as a general (weak) acid catalyst. If the solid contained a significant amount of 'strong' acid sites these would be immediately converted into hydrated protons (water leveling effect) [3] and thus become inactive as heterogeneous catalytic sites. The HET contribution manifests itself within some pH window, on the one hand, where H concentration (and thus the homogeneous rate) is low enough, and on the other, the OH concentration is not too high to compete with the substrate for the acid surface groups.

The critical assumption concerns the step preceding the proton transfer, i.e. the surface proton desorption–adsorption. In homogeneous catalysis this is generally taken as a fast, equilibrated step, the (acidity) constant of which is involved in the well-known Brønsted relationship [3–5,15]. This holds for constant pH heterogeneous runs but might very well not be the case with variable pH ones, for the main reason that the observed pH variations, triggered by continuous or jump amounts of either acid or base added, are supposedly due to proton sorption processes. However, for our purposes the assumption of a quasi-equilibrated surface protonation–deprotonation will be adopted, which requires that the proton transfer to the substrate is rate determining and thus completes the analogy with general acid homogeneous catalysis.

The two-step mechanistic sequence for the heterogeneous route thus reads:

$$(1')\ \mathrm{SH} \rightleftharpoons \mathrm{S} + \mathrm{H};\ K_a = \frac{[\mathrm{S}][\mathrm{H}]}{[\mathrm{SH}]}$$

$$(2')\ \mathrm{SH} + \mathrm{A} \rightarrow \ldots \text{ prod};\ k$$

Here again, kinetically insignificant steps following the rds have been omitted. $K_a$ stands for the surface acidity constant and $k$ for the proton transfer rate constant. The reaction rate along the heterogeneous route is:

$$r_{het} = -(\mathrm{d}[\mathrm{A}]/\mathrm{d}t)_{het} = k[\mathrm{A}][\mathrm{SH}] = (k/K_a)[\mathrm{S}][\mathrm{H}][\mathrm{A}] \quad (1')$$

which after the introduction of the total surface site concentration, $L$,

$$L = [\mathrm{SH}] + [\mathrm{S}] \quad (5)$$

becomes:

$$r_{het} = \frac{Lk}{K_a + [\mathrm{H}]}[\mathrm{H}][\mathrm{A}] = k_{het}[\mathrm{H}][\mathrm{A}] \quad (1'')$$

The overall rate equals the contribution of the two routes, $r = r_{hom} + r_{het}$. At constant pH, the corresponding integral kinetic equation reads:

$$\ln\beta = [\mathrm{H}]\left(\frac{k_0}{K_0} + \frac{Lk}{K_a + [\mathrm{H}]}\right)(t-\tau) = [\mathrm{H}](k_{hom} + k_{het})(t-\tau) = (\kappa_{hom} + \kappa_{het})(t-\tau) \quad (2')$$

so that separation between the two contributions is straightforward. At variable pH it becomes:

$$\ln\beta = k_{hom}\int_{\tau}^{t} h(t)\,\mathrm{d}t + \int_{\tau}^{t} k_{het}(t)h(t)\,\mathrm{d}t = k_{hom}H(t) + k\Theta(t) \quad (4')$$

with $\Theta(t)$ given by:

$$\Theta(t) = L\int_{\tau}^{t} \theta(t)\,\mathrm{d}t \quad (6)$$

and $\theta(t)$, the 'proton fractional surface coverage':

$$\theta(t)=\frac{h(t)}{K_a+h(t)} \quad (7)$$

If, in addition to the above, $K_a \gg h(t)$ over the whole pH range investigated so that $1/(K_a+h(t))$ is slowly varying over the time range $(t-\tau)$, then Eq. 4′ further simplifies to:

$$\ln\beta \approx (k_{hom}+k_{het})\, H(t) \quad (4'')$$

where Eqs. 1′ and 4 have been taken into account. At constant pH Eqs. 4′ and 4″ readily yield Eq. 2′. The more common notation:

$$k_1 = k_{hom}+k_{het}$$
$$= (k_{hom}+k_{het})[H];\ k_2 = k_{hom}+k_{het} \quad (8)$$

designates the observed (overall) first-order, $k_1$, and second-order, $k_2$, rate constants.

Linear plots of $\ln\beta$ vs. $H(t)$ for variable pH homogeneous runs support the '$A_1$' mechanism and provide a convenient means of evaluating $k_{hom}$. For heterogeneous runs this is no longer expected and linear plots may only hold over restricted pH ranges (although the assumed two-step mechanisms still hold), because of the pH variation of $k_{het}$, given by (1″).

As is common in interpreting spectrophotometric data, the value of the endpoint for first-order kinetics is critical [20]. The time-scale of the chosen reaction allows for its end to be reached within the duration of a typical run. However, due to the possible occurrence of some secondary processes affecting endpoint readings, these were checked by means of both fitting procedures [17] and the KMS (Kezdy–Mangelsdorf–Swinbourne) [21] method which was modified to meet the requirements of the specific system under investigation. Within the new approach generated by this application, we were able to discriminate between the HOM and HET contributions to the observed reaction kinetics, provided they are first-order.

The method [21] essentially consists in plotting an earlier portion of the experimental data against a later, constant time lag retarded portion. Thus, denoting this lag by $\Delta t$, Eqs. 2 and 4′ readily yield:

$$\ln\frac{\beta(t+\Delta t)}{\beta(t)} = \ln\frac{a(\infty)-a(t)}{a(\infty)-a(t+\Delta t)}$$
$$= k_{hom}\int_t^{t+\Delta t} h(t)\,dt + Lk\int_t^{t+\Delta t}\theta(t)\,dt \quad (9)$$

In contrast with usual first-order decays, both integrals in Eq. 9 are time-dependent, i.e. they depend not only on $\Delta t$, but also on $t$. For homogeneous runs:

$$\ln\eta(t,\Delta t) = k_{hom}H(t,\Delta t) \quad (10)$$

with

$$\eta=\eta(t,\Delta t)=\frac{a(\infty)-a(t)}{a(\infty)-a(t+\Delta t)}$$
$$=\frac{\beta(t+\Delta t)}{\beta(t)} \quad (11)$$

and

$$H(t,\Delta t)=\int_t^{t+\Delta t} h(t)\,dt = H(t+\Delta t)-H(t) \quad (12)$$

Eq. 10 offers an additional means of evaluating the HOM intrinsic rate constant. It predicts straight-line plots passing through the origin with slope $(k_{hom})$, independent of the time lag. If, in addition, the pH is constant we get, from Eqs. 10–12 and 2:

$$a(t)=a(t+\Delta t)\exp(\kappa_{hom}\Delta t)$$
$$+a(\infty)(1-\exp(\kappa_{hom}\Delta t)) \quad (13)$$

i.e. the usual form of the KMS equation [17]. Its counterpart for constant pH heterogeneous experiments is obtained by taking into account Eq. 2′:

$$a(t)=a(t+\Delta t)\exp((\kappa_{hom}+\kappa_{het})\Delta t)$$
$$+a(\infty)[1-\exp((\kappa_{hom}+\kappa_{het})\Delta t)] \quad (14)$$

Plotting $a(t)$ against $a(t+\Delta t)$ not only yields the (apparent) first order rate constant from the slope of Eqs. 13 or 14, but also allows for the evaluation of the endpoint value, $a(\infty)$. This can be done by either using the corresponding inter-

cepts for some fixed value of $\Delta t$, or as the common intersection point of the straight lines pertaining to different values of $\Delta$t. The overall first-order kinetic behavior in HET runs at constant pH can be more conveniently checked by means of the following equation, which can be obtained from Eqs. 2, 2′, and 11, or from 7 and 9 with $h(t) = [H] = \text{const.}$:

$$\ln\eta(t,\Delta t) = \ln\frac{\beta(t,\Delta t)}{\beta(t)} = [H](k_{hom} + k_{het})\Delta t \quad (15)$$

Once the homogeneous contribution has been determined in a separate experiment, Eq. 15 readily yields the heterogeneous one, $k_{het}$, if any.

The addition of base to the (quasi)equilibrated suspension results in an action similar to that of a 'proton vacuum pump'. The surface proton release which follows:

$$SH \rightarrow S + H$$

can be described in terms of a simple balance equation [8,9]. The charge conservation [8] requires:

$$[Na] + [H] = [S] + [OH] \quad (16)$$

where square brackets designate concentrations of dissolved species, with the exception of the free surface sites S, whose concentration is expressed, as if it were a 'solute', in the same units (i.e. moles/l) by means of the relation [7]:

$$[S] = m\{S\}/V \quad (17)$$

where m is the solid sample mass, $\{S\}$ the 'solid' concentration of S (moles/gram) and $V$ the total liquid phase volume. The time varying surface coverage is given by:

$$\theta = \frac{[SH]}{[SH] + [S]} = 1 - \frac{[S]}{L}; \qquad \theta(t) = 1 - \frac{s(t)}{L} \quad (18)$$

with the same convention (similar to Eq. 17) taken for [SH] and $L$ and $s(t)$ denoting the time-dependent value of [S]. Expressing now the charge balance, 16, in terms of measurable quantities we get:

$$[S] = C_b V_b/(V_b + V_0) + ([H] - [OH]) \quad (19)$$

where $C_b$ and $V_b$ are the analytical concentration and volume of base added, and $V_0$ the initial volume of the solution. The recorded pH thus provides the information needed for evaluating $s(t)$ at any time during the kinetic run. The only unknown quantity remains $L$, which can be retrieved by the following procedure.

Combining Eqs. 18 and 9 and taking into account 11–12 results in:

$$\ln\eta(t,\Delta t) = k_{hom}H(t,\Delta t) + kL\Delta t - kS(t,\Delta t) \quad (20)$$

with $S(t,\Delta t)$ given by:

$$S(t,\Delta t) = \int_t^{t+\Delta t} s(t)\,dt = S(t+\Delta t) - S(t) \quad (21)$$

in which, by analogy with the previously defined proton integral, the function $S(t)$ could be termed 'free site integral'. $k_{hom}$ is determined in separate HOM experiments, whereas $\eta$, $H$, and $S$ are calculated from the HET run data. Defining:

$$y(t,\Delta t) = [\ln\eta(t,\Delta t) - k_{hom}H(t,\Delta t)]/\Delta t; \quad x(t,\Delta t) = S(t,\Delta t)/\Delta t \quad (22)$$

Eq. 20 becomes:

$$y(t,\Delta t) = -kx(t,\Delta t) + kL \quad (23)$$

Eq. 23 is the final expression of the initial mechanistic assumptions, the adopted way of 'charge accounting' and the modified KMS approach. It predicts a linear relation between quantities $y$ and $x$, both derivable from experimental data. The slope of this straight line yields the mechanistic heterogeneous rate constant, $k$ (i.e. the specific rate of the proton transfer from the solid surface sites to the substrate), whereas its intercept provides the value of $L$, the 'bulk' concentration of the active surface acid sites. A simple inspection reveals that the left-hand side adimensional $y$ actually represents the HET contribution to the

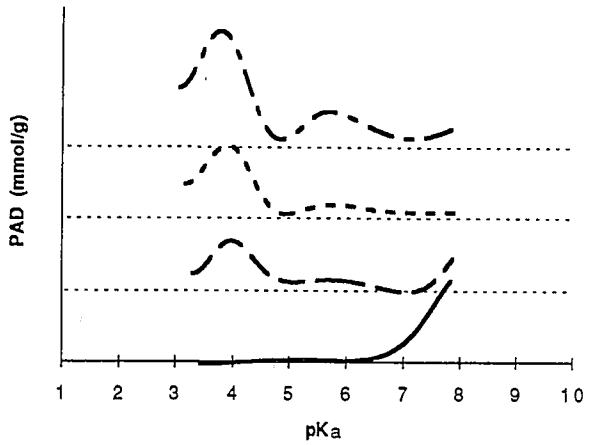


Fig. 2. Proton affinity distributions of the oxide samples. (– – –) 10% AlSi; (– – –) 7% AlSi; (– – –) 3% AlSi; (—) 0% AlSi.

observed first-order decay (the HOM variable pH one, given by Eq. 10, being subtracted). The right-hand side contains only quantities related to the solid sample, i.e. $L$, $k$, and differences of time-dependent free site integral's values. There are several simplifying assumptions embodied in this equation, of which we are fully aware. Extended linear $y(t, \Delta t) - x(t, \Delta t)$ plots are not expected over the whole experimental range investigated. However, the occurrence of such linear behavior, even within restricted ranges, allows for the estimation of two important quantities: $L$, the solid surface concentration of acid sites and $k$, their specific rate of proton transfer. With $L$ expressed in (mol/g) and concentrations in (mol/l) the rate constant, k, units are (g/mol·min). If L is expressed in (mol/m$^2$) via the measured surface area, the units of $k$ become (m$^2$/mol·min).

## 4. Results and discussion

### 4.1. Proton affinity distributions (PAD)

The PADs for silica and the three alumina–silica samples, presented in Fig. 2, were truncated within the pH window of interest here; for clarity they were shifted on the ordinate and spaced by 0.3 mmol/g. As previously reported [22], silica exhibits only 'one type' of acid site as evidenced by a single peak centered around $pK_a \approx 8$ and ascribed to the silanol groups. These are most probably inert as proton donors within the 4.0–7.0 pH window of interest here. By contrast, silica–alumina PADs show several maxima of which two, located at $pK_a \approx 4$ and $pK_a \approx 5.5$, signal the presence of potentially active acid surface sites. They have different weights that change with the alumina content (the second one's contribution increases with Al concentration). Decomposing the affinity spectrum with Gaussian functions was used in order to identify the occurrence of different categories of surface Brønsted sites (qualitative characterization) and to isolate their contribution to the total proton binding curve (quantitative characterization). In this step we used the Peakfit® software (Jandel Scientific) and the quality of the fit was judged from the values of standard deviation and correlation coefficient. As additional constraints, we preferred fits with the minimum possible number of components and rejected those fits where the Gaussian half-width exceeded 0.75 p$K$ units. The later limit was found from separate experiments with simple model compounds, as described elsewhere [23].

Table 1
PADs results

| Sample | $pK_a^I$ | $pK_a^{II}$ | $L^I$ mmol/g | $L^{II}$ mmol/g |
|---|---|---|---|---|
| 0% $Al_2O_3/SiO_2$ | | 8.2 | | 0.605 |
| 3% $Al_2O_3/SiO_2$ | 4.0 | 5.7 | 0.217 | 0.06 |
| 7% $Al_2O_3/SiO_2$ | 3.8 | 5.7 | 0.345 | 0.056 |
| 10% $Al_2O_3/SiO_2$ | 3.8 | 5.7 | 0.528 | 0.104 |

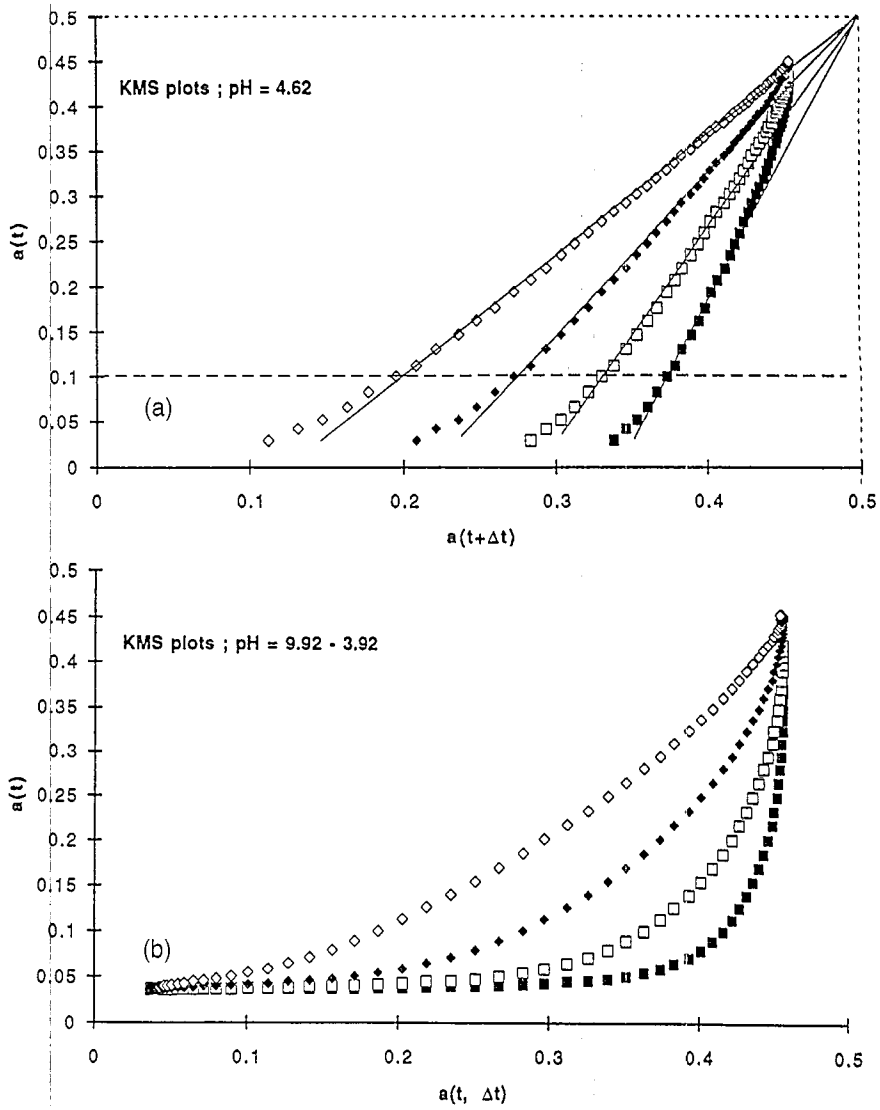


Fig. 3. KMS plots for homogeneous runs: (a) constant pH; (b) variable pH (■) $\Delta t$=8 min; (□) $\Delta t$=6 min; (♦) $\Delta t$=4 min; (◇) $\Delta t$=2 min.

The calculated site concentrations within their respective pH windows are presented in Table 1.

### 4.2. Homogeneous experiments

Several constant and variable pH runs were necessary to establish the reaction behavior and to obtain $k_{hom}$. Fig. 3a contains a typical constant pH KMS plot (Eq. 13). For all values of $\Delta t$ linearity is obeyed after a time delay needed for reactant dispersion throughout the reaction volume. Due to some secondary processes, the final readings also fall off the straight lines which converge to an endpoint absorbance value around 0.5. (As a rule, endpoint values of HOM runs are larger than the corresponding HET ones. This is due either to some strongly adsorbed amount of reactant or product on the solid surface or to the enhancement of the secondary processes). Pseudo first-order rate constants, $\kappa_{hom}$, are calculated from the linear parts of KMS plots (see Eq. 13); their ratio to the constant [H] (see Eq. 2′) then yields the intrinsic constants, $k_{hom}$. To avoid as much as possible the

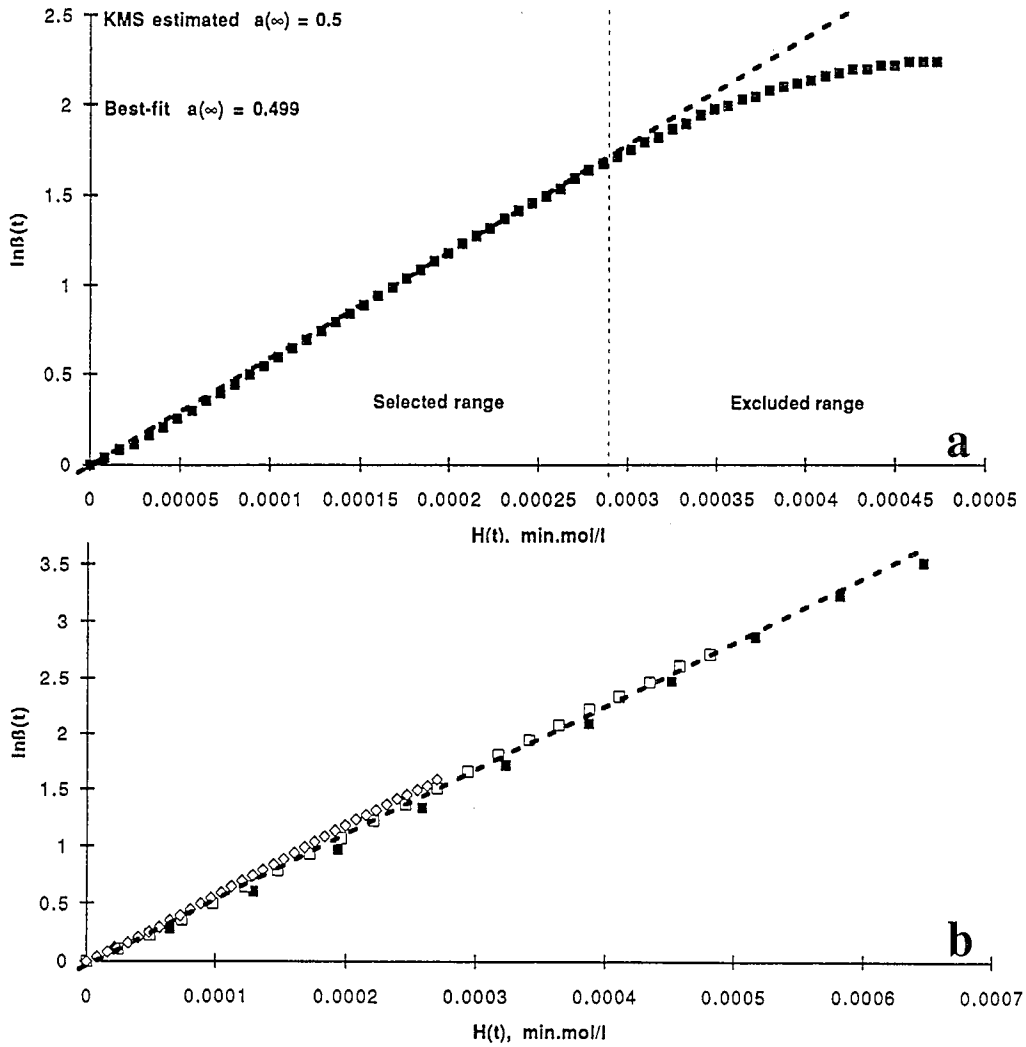


Fig. 4. Constant pH HOM runs: (a) graphical domain selection; (b) best-fit endpoints plots (■) pH = 4.19; $a(\infty) = 0.495$; $k_{hom} = 5644$ l/mol·min; (□) pH = 4.62; $a(\infty) = 0.487$; $k_{hom} = 5817$ l/mol·min; (◆) pH = 6.22; $a(\infty) = 0.505$; $k_{hom} = 6052$ l/mol·min; (◇) pH = 4.62; $a(\infty) = 0.499$; $k_{hom} = 6025$ l/mol·min.

arbitrariness in selecting a specific value, the following procedure was adopted.

KMS plots were used as first estimates of rate constant and endpoint ($a(\infty)$) values. Next, plots of $\ln\beta(t)$ against $H(t)$ (see Eq. 4) were constructed using the estimated endpoints. Recall, for constant [H] the proton integral simply replaces the time variable and the slope of plots such as that represented in Fig. 4a directly gives the intrinsic constant, $k_{hom}$. The linear portion is used in subsequent data processing, which involves determining the endpoint with the best fit of the straight-line [24]. The resulting plots for four different runs at different pH values are given in Fig. 4b; the differences of 4% in endpoint and 7% in rate constant values can be considered as lying within reasonable error limits.

Variable pH runs (simulating the pH decrease of HET ones) were performed with the microburet's lowest dosing rate (5 μl/min $HNO_3$ 0.1 N) which resulted in pH variation rates slightly higher than the ones observed in HET experiments. Typical KMS plots, as shown in Fig. 3b, clearly illustrate the inapplicability of the method in its original form: there are no linear portions and, as $\kappa_{hom} = k_{hom}[H]$ and [H] is a function of time,

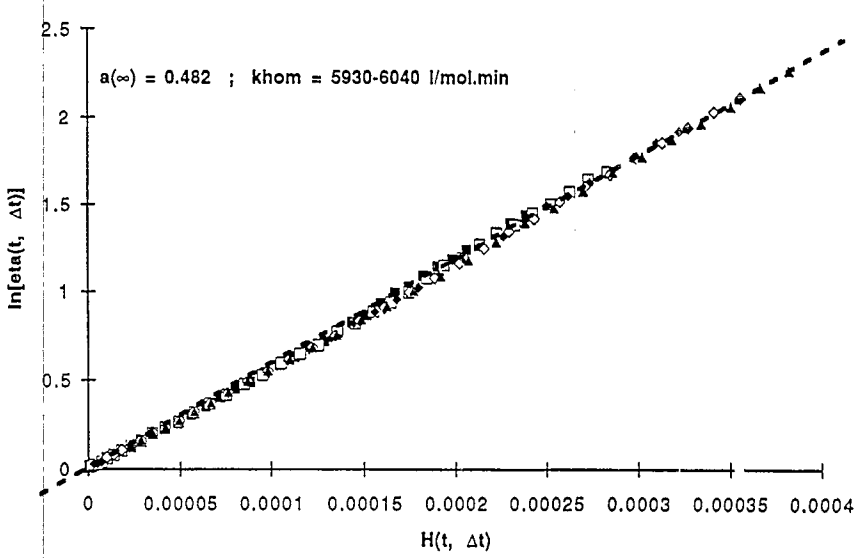


Fig. 5. Variable pH HOM run. (■) $\Delta t$=4 min; (□) $\Delta t$=5 min; (♦) $\Delta t$=6 min; (◇) $\Delta t$=7 min; (▲) $\Delta t$=8 min.

straight-line plots are not even expected. If the mechanism is not changing under the induced proton concentration variation, linear plots such as those predicted by Eq. 4 or its equivalent, Eq. 10, are expected and were obtained, as shown in Fig. 5, in which the later alternative was preferred. Thus the '$A_1$' mechanism for the HOM route is preserved even in the case of variable homogeneous catalyst concentration. Subtracting the contribution of this route from the variable pH HET runs as illustrated in Eq. 22 is therefore justified. The proton integral, or constant delayed differences in its values, $H(t, \Delta t)$, replace the more familiar time quantities, $t$ and $\Delta t$, and the corresponding slopes directly yield the intrinsic rate constant ($k_{hom}$). Values of the latter lying within 5500–6500 l/mol·min were obtained in variable pH runs, using the final absorbance reading as endpoint. As mentioned, this is the critical quantity in first-order kinetics and probably the main source of error in our experiments.

Fig. 6 illustrates the influence of the endpoint on the rate constant, obtained as the slope of straight-lines as in Fig. 5, for a variable pH run.

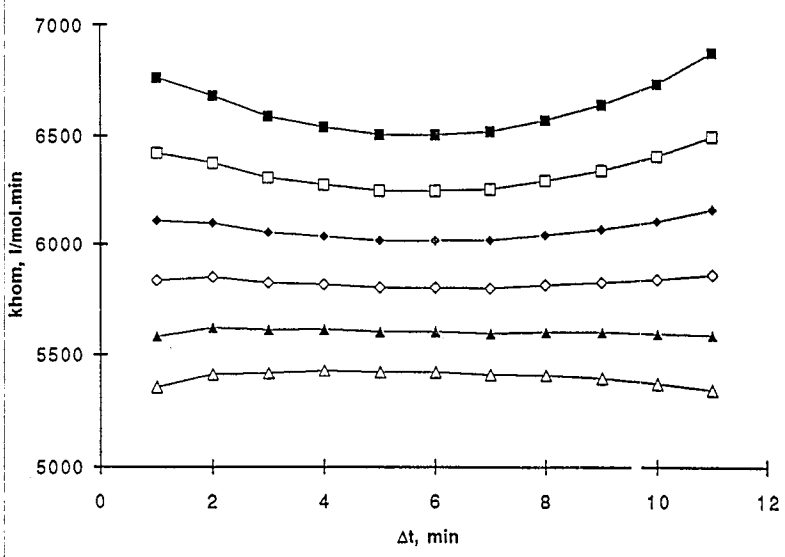


Fig. 6. Variable pH HOM run: endpoint influence on the rate constant. (-■-) $a(\infty)$ = 0.470; (-□-) $a(\infty)$ = 0.475; (-♦-) $a(\infty)$ = 0.480; (-◇-) $a(\infty)$ = 0.485; (-▲-) $a(\infty)$ = 0.490; (-△-) $a(\infty)$ = 0.495.

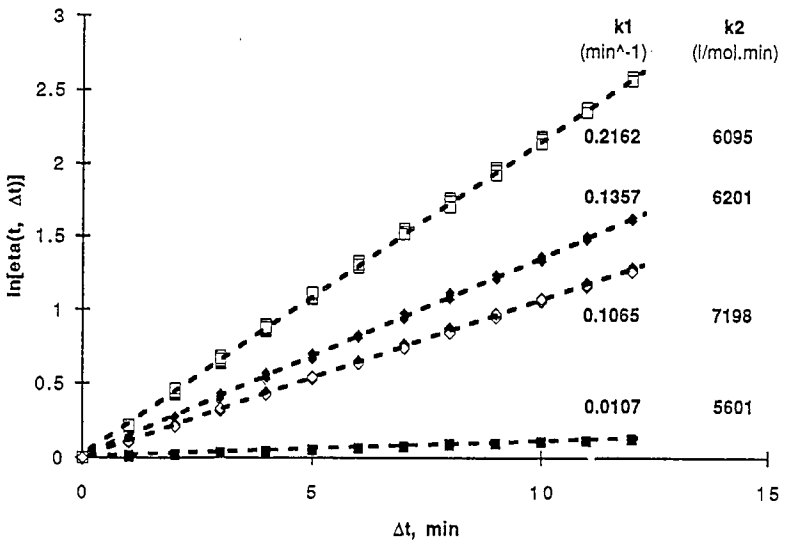


Fig. 7. Quasi-constant pH HET runs, (■) 0% AlSi; pH = 5.72; (□) 3% AlSi; pH = 4.45; (♦) 7% AlSi; pH = 4.66; (◇) 10% AlSi; pH = 4.83.

For differences in endpoint values of about 5% the corresponding differences in the rate constants may exceed 15%, depending also on the $\Delta t$ value. This is the reason why best-fit values were preferred whenever this was possible (i.e. HOM and constant pH HET experiments). This implicitly involves the overall first-order kinetics as 'certain', which is consistent with the assumed mechanisms of the two reaction routes. An average value of $6 \cdot 10^3$ l/mol·min was taken for the homogeneous intrinsic rate constant and subsequently used to evaluate the heterogeneous one in both constant and variable pH runs.

### 4.3. Constant pH heterogeneous experiments

KMS plots are similar to those presented in Fig. 3a (HOM runs), with the exception that the extrapolated endpoint values are slightly lower, which also holds true for the experimental final absorbance readings. The most important difference occurs in the case of pure silica, where strong 'trapping' of the organic components is responsible for their lower concentration in solution, detected spectrophotometrically. Silica thus appears more as an inhibitor than as a catalyst, even if this is due to the secondary effect of strong

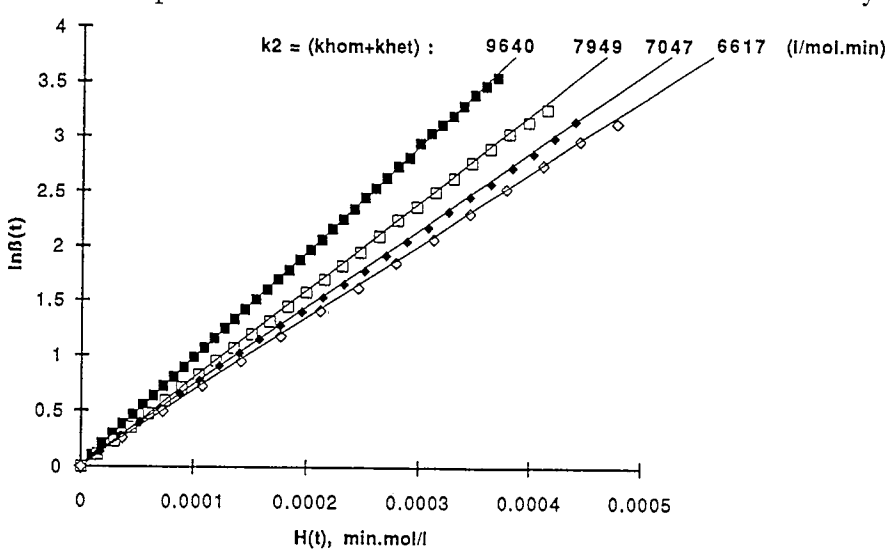


Fig. 8. 10% $Al_2O_3/SiO_2$ quasi-constant pH HET runs. (■) pH = 5.04–4.99; $a(\infty) = 0.465$; (□) pH = 4.82–4.77; $a(\infty) = 0.469$; (♦) pH = 4.77–4.72; $a(\infty) = 0.448$; (◇) pH = 4.44–4.48; $a(\infty) = 0.486$.

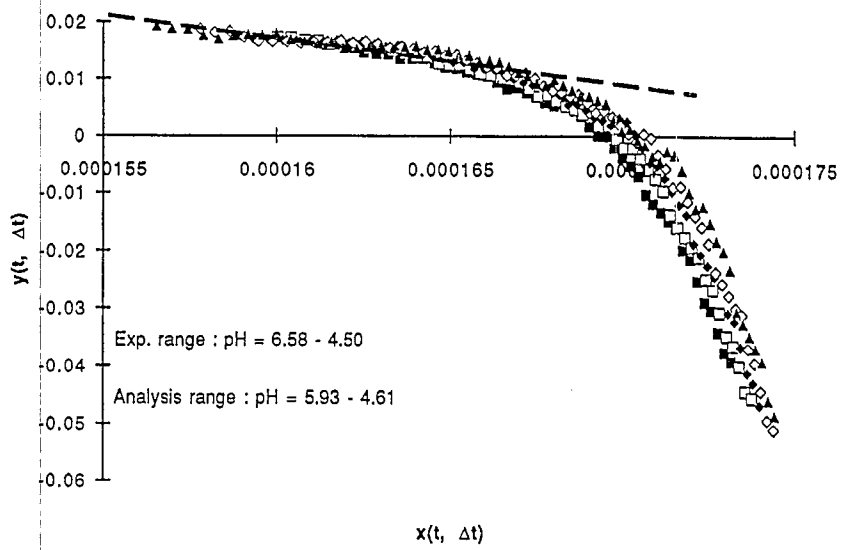


Fig. 9. 3% $Al_2O_3/SiO_2$: $x$–$y$ plot for variable pH HET run. (■) $\Delta t = 16$ min; (□) $\Delta t = 14$ min; (♦) $\Delta t = 12$ min; (◇) $\Delta t = 10$ min; (▲) $\Delta t = 8$ min.

adsorption and not to the altering of some of the mechanistic steps. In fact, its true HET contribution is negligible, in agreement with its PAD spectrum which shows no 'active' acid sites within the pH window of interest here.

Linear plots, predicted by Eqs. 2′ and 15, were obtained within extended experimental ranges for HET runs, with all the solid samples investigated. Such behavior, pertaining to the D domain of Fig. 1, is shown in Fig. 7, the HET counterpart of Fig. 5; this clearly supports the mechanistic assumptions involved in the kinetic analysis. However, for comparative purposes constant pH experiments are not the best experimental alternative. Rigorously constant pH is difficult to attain and even more difficult to reproduce with different samples. As these exhibit different surface coverages of different types of acid sites, depending on the working pH, the corresponding $k_{het}$ contributions are not convenient quantities for comparison. This is evidenced in Fig. 7, which displays sizable differences in the intrinsic rate constant

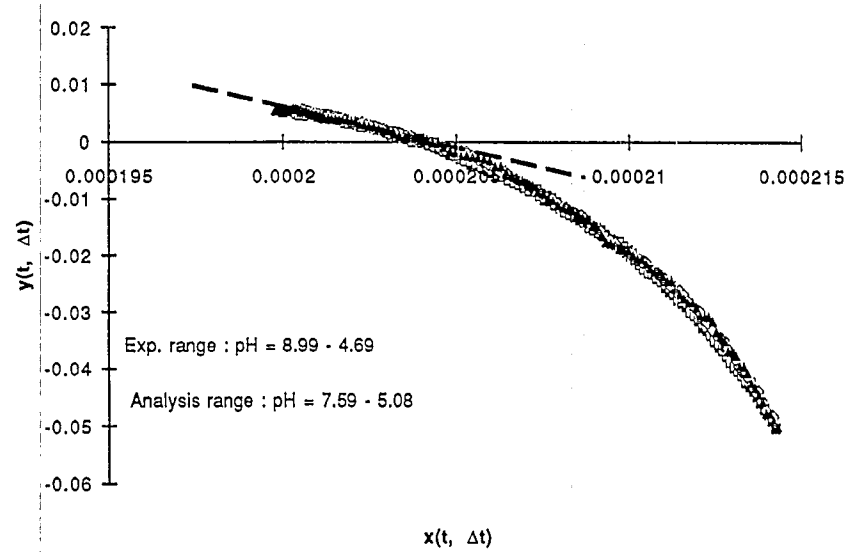


Fig. 10. 7% $Al_2O_3/SiO_2$: $x$–$y$ plot for variable pH HET run. (■) $\Delta t = 16$ min; (□) $\Delta t = 14$ min; (♦) $\Delta t = 12$ min; (◇) $\Delta t = 10$ min; (▲) $\Delta t = 8$ min.

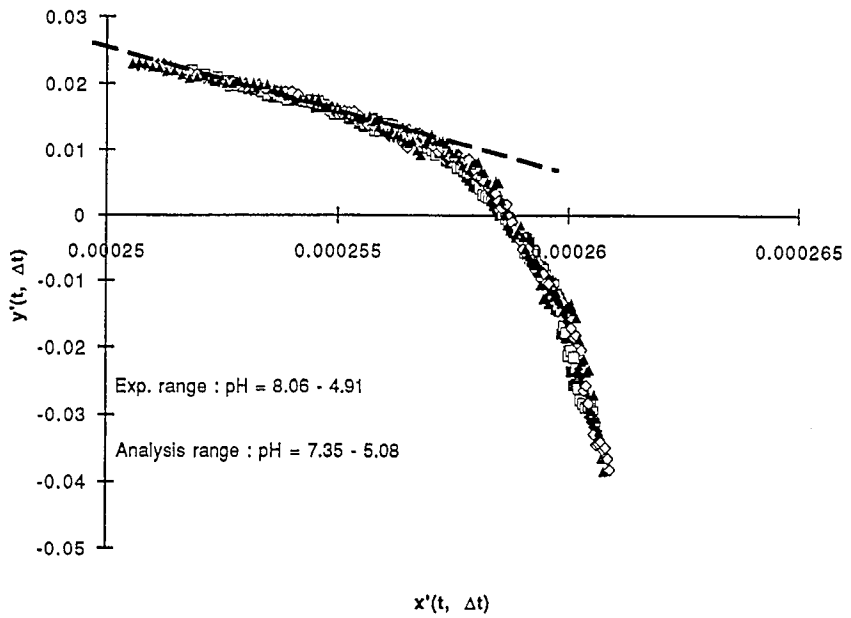


Fig. 11. 10% $Al_2O_3/SiO_2$: $x$–$y$ plot for variable pH HET run. (■) $\Delta t = 16$ min; (□) $\Delta t = 14$ min; (♦) $\Delta t = 12$ min; (◇) $\Delta t = 10$ min; (▲) $\Delta t = 8$ min.

only in the case of the 10% sample, within a favorable pH window. For the latter sample a significant variation of the rate constant is presented in Fig. 8, which illustrates the application of Eq. 2′ for constant pH runs. The observed behavior, i.e. the decrease of the HET contribution with lowering of the pH, supports the basic idea of the preceding section: the heterogeneous contribution is not expected at higher proton concentrations, where the reaction proceeds only through the homogeneous route.

The numerical values obtained are open to discussion. The proton transfer rate constant given by Eq. 2′ is $k = k_{het}(K_a + [H])/L$; with $K_a$ and $L$ estimated by means of the proton affinity distributions the $k_{het}$ values of Fig. 8 can be used to calculate $k$. However the PAD spectrum of Fig. 2 reveals two types of acid sites, denoted I and II, and located at $pK_a^I \approx 4$ and $pK_a^{II} \approx 5.5$, respectively. Within the pH window in which kinetic experiments take place both these sites are able, in principle, to act as proton donors for the organic substrate. The corresponding values of the proton transfer rate constants, expressed in g/mol·min, range between $k^I = 1264$ and $k^{II} = 427$ for pH = 5.02 and $k^I = 244$ and $k^{II} = 227$ for pH = 4.46, with the trend to decrease with pH for both. Such large differences are not reflecting the inherent experimental errors only. They also express the fact that whereas the mobile proton is probably able to access the entire solid surface, the large organic substrate is not. Thus 'site concentrations', as given by PADs, represent upper-limit values while the orthoester is able to 'see' considerably less. This is merely reflected in the dramatic pH-dependent evolution of $k^I$, where increasing of [H] 'hides' the solid surface and drives the reaction to the HOM route. Division by overestimated value of $L^I = 0.528$ mmol/g causes the marked decrease of the corresponding rate

Table 2
Kinetic results

| Sample | $S_{BET}$ $m^2/g$ | $L$ mmol/g | $10^5 \cdot L$ mmol/$m^2$ | $k$ g/mol·min | $10^{-5} \cdot k$ $m^2$/mol·min |
|---|---|---|---|---|---|
| 3%$Al_2O_3$/$SiO_2$ | 330 | 0.085 | 0.256 | 1650 | 4.8 |
| 7%$Al_2O_3$/$SiO_2$ | 260 | 0.101 | 0.387 | 1340 | 3.9 |
| 10%$Al_2O_3$/$SiO_2$ | 270 | 0.131 | 0.484 | 1460 | 4.4 |

constant. For the type II sites, which are 'highly covered' within the above pH range, the effect is attenuated. These numerical estimations pertain to the hypothetical situation where either sites of type I alone, or sites of type II alone, were present on the surface. In fact, they coexist and both cooperate in the catalytic reaction; thus the observed intrinsic HET contribution, $k_{het}$, represents an average quantity. These complications, occurring for a single sample, illustrate the above assertion that constant pH measurements are inadequate for comparative purposes. A large number of 'pH narrowly spaced' runs would be necessary to solve such ambiguities and discriminate between different samples. The required $\Delta$pH diminution between two successive runs leads to the idea of using a single pH-drift experiment to obtain (independently) average values of $k$ and $L$.

### 4.4. Variable pH heterogeneous experiments

Typical $x$–$y$ plots, obtained by applying Eq. 23 to variable pH runs for each of the $Al_2O_3/SiO_2$ samples are presented in Figs. 9-11. As mentioned, the predicted linearity does not hold for the whole experimental range. All plots bend after an extended initial linear portion and this coincides with the increase in the scatter of points. This may be attributed to both experimental errors (absorbance readings differences, embodied in $y$, decrease markedly with the reaction approaching its end) and to the existence of two types of active sites, mentioned above. However the 'tightness' of the first domain for different values of $\Delta t$ definitely supports the basic mechanistic assumptions. One should notice that the first (linear) part of $x$–$y$ plots corresponds to the higher pH range, i.e. to the zone where the HET catalytic effect has a sizable contribution.

The classical KMS method was generalized [25] and its optimization further analyzed [26] in terms of a detailed statistical approach, noise correction and simulated applications pertaining to the common first-order decay ($y(t) = A\exp(-kt) + Z$). Their extension to the case presented here, in which the generalization of the first-order equation itself took place, is not straightforward. The two main prescriptions [26] concerning the time-lag and points selection were, however, followed. First, recorded experimental points were used only once within the selected linear domain (although some of them were used twice in representing the entire $x$–$y$ plots). This was consistent with the idea of selecting the initial part of the reaction, where the contribution of secondary processes is minimal. Second, the time-lags used in the calculation of $k$ and $L$ represented approximately 25% of the analysis domain, although several values were used in Figs. 9-11 for illustration. More scattered plots and poorer correlation coefficients (exceeding 0.95, however) were thus preferred in order to avoid biased results.

An important feature of Eq. 23 is the fact that $k$, the specific solid-substrate proton transfer rate, is a factor in the right-hand side. That means that experimental errors, mainly those due to the endpoint determination, will be reflected in the $k$ and not in the $L$ values. Kinetic scanning runs are thus expected to offer reliable values of active surface acid sites' concentrations. To reduce the endpoint influence, the same value, $a(\infty) = 0.48$ was used in Eq. 23 for all variable pH runs. This is consistent with the already mentioned lower values observed in all HET experiments and with the corresponding constant pH KMS plots. Simulated variations in endpoint values resulted in appreciable variations in $k$ but not in $L$, both given in Table 2 for $a(\infty) = 0.48$ and time-lag values, $\Delta t$, around one fourth of the selected time domain for each run. Both experimental and analysis domains are given in pH units (more suggestive than time units) in Figs. 9-11.

The most important feature of the values presented in Table 2 concerns those of $L$. As mentioned, these have to be regarded as average concentrations of acid sites accessible to the organic substrate. They lie in the expected order for the samples investigated, i.e. increase with the aluminum content, and range between those estimated by PADs, i.e. are lower than the type I sites and higher than type II sites concentrations, given

in Table 1. The site concentrations determined here agree with those reported by Sato et al. [27] on silica–alumina. Their values, obtained by DMP (2,6-dimethylpyridine) adsorption range within 0.058–0.126 mmol/g for a series of different samples. The $k$ values, although exhibiting some differences, may be considered as practically identical in view of the fact that they include most of the experimental errors.

## 5. Conclusions

A detailed kinetic analysis accounting for concomitant homogeneous specific and heterogeneous general acid catalyzed reactions has been presented, in relation to the hydrolysis of a specific orthoester. There is a pH window which allows for separation of the two processes and which is conditioned by the acidic properties of the solid oxides that function as heterogeneous catalysts. Solid surface proton binding distributions, obtained by potentiometric titration in the absence of the organic reagent, revealed the suitable pH range for kinetic study. Two types of acid sites likely contributed to the heterogeneous route of the reaction; they were located at $pK_a^I \approx 4$ and $pK_a^{II} \approx 5.5$ on the acidity scale. The total concentration of type I potentially active sites, as revealed by proton affinity distributions, increased with the aluminum content and always exceeded the actual value, determined through kinetic scanning.

## Acknowledgements

This work was supported by the National Science Foundation under Grant NSF No. CHE 9319593.

The authors also acknowledge the experimental contributions of Mr. Gino Duca.

## References

[1] B.C. Gates, Catalytic Chemistry, John Wiley & Sons, New York, 1992.
[2] J.N. Brønsted, Rec. Trav. Chim., 42 (1923) 718.
[3] R.P. Bell, The Proton in Chemistry, Chapman and Hall, London, 1973.
[4] E. Caldin and V. Gold (Eds.), Proton-Transfer Reactions, Chapman and Hall, London, 1975.
[5] R. Stewart, The Proton: Applications to Organic Chemistry, Academic Press, London, 1985.
[6] J.H. Clark, Catalysis of Organic Reactions by Supported Inorganic Reagents, VCH, New York, 1994.
[7] H.H. Kung, in B. Delmon and J.T. Yates (Eds.), Transition Metal Oxides: Surface Chemistry and Catalysis, Studies in Surface Science and Catalysis, Vol. 45, Elsevier, Amsterdam, 1989.
[8] P.W. Schindler and W. Stumm, in W. Stumm (Ed.), Aquatic Surface Chemistry; Chemical Processes at the Particle–Water Interface, John Wiley & Sons, New York, 1987, Chapter 4.
[9] C. Contescu, J. Jagiello and J.A. Schwarz, Langmuir, 9 (1993) 1754.
[10] C. Contescu, J. Hu, and J.A. Schwarz, J. Chem. Soc., Faraday Trans., 89 (1993) 4091.
[11] C. Contescu, V.T. Popa, and J.A. Schwarz, J. Catal., in press, 1995.
[12] C.J. Brinker and G.W. Sherer, Sol–Gel Science – The Physics and Chemistry of Sol–Gel Processing., Academic Press, San Diego, CA, 1990.
[13] R.J. Stol, A.K. Van Helden and P.L. De Bruyn, J. Colloid Interface Sci., 57 (1976) 115.
[14] H.H. Kung, J. Solid State Chem., 52 (1984) 191.
[15] E.H. Cordes and H.G. Bull, Chem. Rev., 74 (1974) 581.
[16] R. Durand, P. Geneste, C. Moreau and S. Mseddi, Stud. Surf. Sci. Catal., 20 (1985) 319.
[17] K.A. Konnors, Chemical Kinetics. The Study of Reaction Rates in Solution, VCH Publishers, New York, 1990.
[18] D. French, J. Am. Chem. Soc., 72 (1950) 4806.
[19] S. Widequist, Acta Chem. Scand., 4 (1950) 1216.
[20] W.P. Jencks, Catalysis in Chemistry and Enzymology, Dover Publications, New York, 1987.
[21] F.J. Kezdy, J. Jaz, A. Bruylants, Bull. Soc. Chim. Belg., 67 (1958) 687; P.C. Mangelsdorf, J. Appl. Phys., 30 (1959) 442; E.S. Swinbourne, J. Chem. Soc., 2371 (1960).
[22] C. Contescu, A. Contescu and J.A. Schwarz, Progr. Catal., 2 (1993) 1.
[23] T.J. Bandosz, J. Jagiello, C. Contescu, and J.A. Schwarz, Carbon, 31 (1993) 1193.
[24] R.C. Williams and J.W. Taylor, J. Chem. Educ., 42 (1970) 129; M.J.J. Holt and A.C. Norris, J. Chem. Educ., 54 (1977) 426.
[25] L.M. Schwartz, Anal. Chem., 53 (1981) 206.
[26] G.H. McKinnon, C.J. Backhouse, and A.H. Kalantar, Int. J. Chem. Kinet., 16 (1984) 1427.
[27] S. Sato, M. Hiratsuka, T. Sodesawa and F. Nozaki, Bull. Chem. Soc. Jpn., 64 (1991) 2214.